Shape evolution in Kr, Zr and Sr isotopic chains in covariant density functional theory.

H. Abusara[1,*] and Shakeb Ahmad[2,†]

[1] *Department of Physics, Birzeit University, Birzeit, Palestine*
[2] *Physics Section, Women's College, Aligarh Muslim University, Aligarh - 202002, India.*

(Dated: December 4, 2017)

The relativistic-Hartree-Bogoliubov formalism using density-dependent zero and finite range N-N interactions, and separable pairing, is applied to the Kr isotopes (Z = 36) and N = 34 - 64 isotopes, neutron-rich Sr(Z=38) and Zr(Z=40) nuclei with neutron numbers N=48-70. A systematic search of triaxial ground state and the phenomena of unusual structural change and the coexistence of shape for $^{70-100}$Kr, and at N=58 in the $^{86-108}$Sr and $^{88-110}$Zr isotopes are done. A reasonable agreement is found with the available experimental data and with the macro-microscopic finite range droplet model. The findings are also in good agreement with the self-consistent Hartree-Fock-Bogoliubov calculations based on the interaction Gogny-D1S force, and with relativistic calculations.

PACS numbers: 21.60.Jz, 24.75.+i, 27.90.+b

I. INTRODUCTION

The availability of modern radioactive ion beam (RIB) facilities has greatly reinvigorated theoretical as well as experimental interest in investigating new and often exotic nuclear structure phenomena of neutron-rich nuclei throughout the chart of nuclei. Neutron-rich nuclei in the mass region A≈100 of the nucleic chart are of special interest. These neutron-rich nuclei are relevant for the r-process of stellar nucleosynthesis. They show some evidence of unusual features in some of their isotopic chains with an abrupt variation of particular nuclear properties, such as the quadrupole deformation, and show the corresponding phenomena of shape coexistence. Two distinct quantum configurations of nucleons at the very low excitation energy with very different intrinsic properties are interpreted as the phenomena of shape coexistence.

In many neutron-rich isotopes, an extremely abrupt transition in shape and shape coexistence has been observed experimentally [1–7]. Abrupt change of shape from spherical to deformed shape and shape coexistence between spherical and deformed configurations is best seen in the neutron-rich nuclei with $N \approx 60$. Neutron-rich Sr and Zr nuclei are the best candidates to study such phenomena in this region with $N \approx 58$. These effects are attributed to the interplay between the spherical gaps at Z=38, 40, and N=56, 58, and the deformed subshell closures at Z=38, 40, and N=60, 62, and 64. Observation of very low-lying $0_2{}^+$ states is an another unusual feature in this region along with the shape transition. It is interpreted as an evidence for shape coexistence. In recent studies of Sr and Zr nuclei, irregularities in the neutron separation energy, charge radii, and the first 2^+ excited state energy, have provided evidence about unusual abrupt change in the nuclear structure at $N = 60$ [8–10]. An extensive review upon the unified description of shape coexistence in this mass region is presented in Ref. [11] and references therein.

Recently, as reported by research performed at the REX-ISOLDE facility at CERN, the reduced transition probabilities and spectroscopic quadrupole moments manifested experimental evidence for shape coexistence in neutron-rich strontium (^{96,98}Sr) isotopes at $N = 60$ [12]. Another observation of collective structure in the closed-subshell nucleus ^{94}Zr manifested the shape coexistence in ^{94}Zr. The role of subshells for nuclear collectivity is suggested to be important in this case [13]. On the basis of some indirect evidences in the analysis of energy patterns from rotational band [14**?** , 15] and electric monopole transition strength [2, 16–18], possibility of the shape coexistence is suggested in the zirconium (^{94}Zr and ^{100}Zr) isotopes.

In order to understand the exotic features in this mass region, recent as well as earlier experimental data are needed to be fully described and compared. Therefore, different nuclear structure models are aimed in their recent nuclear structure studies at understanding the various unusual structural transitions and effects arising due to the competition between the macroscopic and microscopic degrees of freedom. In this regard, a realistic description of the structural evolution and shape coexistence in Kr, Sr and Zr isotopes has been addressed earlier in many theoretical studies within the different formalisms. Nomura *et al.* in thiet recent study [19] showed the rapid structural change between N=58 and 60 in $^{94-110}$Zr and $^{92-108}$Sr isotopes, within the SCMF-to-IBM mapping procedure based on the Gogny-D1M EDF. In the same framework Nomura *et al.* [20] studied the shape evolution in Kr isotopes, and showed the prolate and oblate shape transitions and shape coexistence on both sides of the isotopic chains. The triple shape coexistence specific for the 0^+ states and the evolution of the shape coexistence and mixing in the neutron-rich $N = 58$ Sr and Zr isotopes are studied within the complex excited VAMPIR approach [21]. A realistic, effective interaction based on the Bonn A potential is used in this approach. In the shell model(SM) framework [22],

* habusara@birzeit.edu(Corresponding author)
† physics.sh@gmail.com

the spherical-to-deformed shape transition in Zr(Z=40) isotopes with neutron numbers from N = 50 to N = 58 is studied using a modest valence space with a ^{78}Ni inert core. In another recent work by J. Xinag *et al.* [23] within the covariant density functional theory (DFT), the coexistence of prolate and oblate shapes is observed in ^{98}Sr and ^{100}Zr. They also found a moderate shape transition in Kr isotopes. However, one takes into consideration that treatment of pairing correlation in [23] is done based on the BCS approximation. In his study, the sharp kink observed in the charge radii at $N = 60$ is shown to be related to the abrupt change in nuclear shapes. Numerous other theoretical studies aiming to understand the structural evolution are done within different formalism. These include the relativistic mean-field (RMF) theory [24, 25], the generator coordinate method (GCM) [26], the interacting boson model(IBM) approximation [27], the VAMPIRE model [28, 29], the macroscopic-microscopic method [**?**], the shell model (SM) [30–36], the Hartree-Fock (HF) and Hartree-Fock-Bogoliubov (HFB) method [37, 38], the Monte Carlo shell model[39].

In the present study, we shall present the numerical results of a systematic calculation in the search of triaxial ground state properties and shape coexistence in the shape coexistence in the neutron-rich Sr(Z=38) and Zr(Z=40) nuclei with neutron numbers N=54-70, and in the Kr (Z=36) isotope chain with N=34-64. The present analysis is an attempt to describe self-consistently the phenomena of unusual structural change and the coexistence of shape in the $^{94-110}$Zr and $^{92-108}$Sr isotopes at N=58, and for the Kr isotopes chain. The systematic constrained triaxial calculation is done in the self-consistent mean field model the relativistic-Hartree-Bogoliubov (RHB) with density-dependent zero and finite range N-N interactions. The model parameter used are the density-dependent point-coupling DD-PC1 [40], and non-linear meson-exchange coupling NL3* [41]. They provide a successful description of ground state properties[42–45] over all the nuclear charts. Pairing correlations are considered in the separable pairing model [46].

This article is organized as follows. In Sec. II a general overview of the RHB formalism is presented. Potential energy surfaces for the three isotopic chains are discussed and compared with the results from others in Sec. III. Bulk properties for the ground state will be discussed in Sec. IV. Summary and conclusions are in Sec. V.

II. THEORETICAL FRAMEWORK

For the present investigation, the self-consistent RHB with density-dependent finite range meson-exchange model and a density-dependent zero-range point-coupling model are used [40, 47–50]. These models provide a very successful and an excellent description of different ground states and excited state properties over the entire nucleic chart [42–45, 47, 51–56]. The present investigation uses the very successful, density-dependent point-coupling DD-PC1 [40], and nonlinear meson-nucleon coupling NL3* [41] parameters.

A. The meson-exchange model

The meson-exchange model is defined by the standard Lagrangian density with medium dependence vertices [57]

$$\begin{aligned}\mathcal{L} &= \overline{\psi}\left[\gamma(i\partial - g_\omega\omega - g_\rho\vec{\rho}\vec{\tau} - eA) - m - g_\sigma\sigma\right]\psi \\ &+ \frac{1}{2}\left(\partial\sigma\right)^2 - \frac{1}{2}{m_\sigma}^2\sigma^2 - \frac{1}{4}\mathbf{\Omega}_{\mu\nu}\mathbf{\Omega}^{\mu\nu} + \frac{1}{2}m_\omega^2\omega^2 \\ &- \frac{1}{4}\vec{\mathbf{R}}_{\mu\nu}\vec{\mathbf{R}}^{\mu\nu} + \frac{1}{2}m_\rho^2\vec{\rho}^2 - \frac{1}{4}\mathbf{F}_{\mu\nu}\mathbf{F}^{\mu\nu}. \end{aligned} \quad (1)$$

where m is the bare nucleon mass and ψ denotes the Dirac spinors. The masses m_σ, m_ω, and m_ρ are those of the σ meson, ω meson, and the ρ meson, with the corresponding coupling constants for the mesons to the nucleons as g_σ, g_ω, g_ρ, respectively, and e is the charge of the proton. These coupling constants and unknown meson masses are the Lagrangian equation.(1) parameters. Here, $\Omega^{\mu\nu}$, $\vec{R}^{\mu\nu}$, and $F^{\mu\nu}$ are the field tensors of the vector fields ω, ρ, and the photon.

This linear model has first been introduced by Walecka [58, 59], however, this simple model does not provide a quantitative description of nuclear system [60, 61] with interaction terms that are only linear in the meson fields. For a realistic description of complex nuclear system properties one can either introduce a nonlinear self-coupling or a density dependence in the coupling constants.

For the nonlinear self coupling, one has to add the following term to the Lagrangian:

$$U(\sigma) = \frac{1}{2}m_\sigma^2\sigma^2 + \frac{1}{3}g_2\sigma^3 + \frac{1}{4}g_3\sigma^4 \quad (2)$$

for scalar mesons this has turned out to be crucial [60]. This model has been successfully used in a number of studies [57, 62–64]. We have used the recently proposed parameter set NL3* [41], which is a modern version of the widely used parameter set NL3 [63]. It improves the description of the ground state properties of many nuclei over parameter set NL3, and provides a simultaneously excellent description of excited states with collective character in spherical as well as in deformed nuclei.

In the case of the density dependent coupling constants one defines the dependence as

$$g_i(\rho) = g_i(\rho_{sat})f_i(x) \quad (3)$$

i can be any of the three mesons σ,ω, and ρ where the density dependence is given by

$$f_i(x) = a_i\frac{1 + b_i(x + d_i)^2}{1 + c_i(x + d_i)^2}. \quad (4)$$

for σ and ω and by

$$f_\rho(x) = \exp(-a_\rho(x-1)). \tag{5}$$

for the ρ meson. x is defined as the ratio between the baryonic density ρ at a specific location and the baryonic density at saturation ρ_{sat} in symmetric nuclear matter. The eight parameters in Eq. (4) are not independent, but constrained as follows: $f_i(1) = 1$, $f_\sigma^{''}(1) = f_\omega^{''}(1)$, and $f_i^{''}(0) = 0$. These constrains reduce the number of independent parameters for density dependence to three. This model is represented in the present investigations by the parameter set DD-ME2 [47].

B. The point-coupling model

The effective Lagrangian density for the density-dependent point-coupling model [40, 65, 66] that includes the isoscalar-scalar, isoscalar-vector, and isovector-vector four-fermion interactions is given by

$$\begin{aligned}\mathcal{L} &= \bar{\psi}(i\gamma.\partial - m)\psi \\ &- \frac{1}{2}\alpha_s(\hat{\rho})(\bar{\psi}\psi)(\bar{\psi}\psi) - \frac{1}{2}\alpha_V(\hat{\rho})(\bar{\psi}\gamma^\mu\psi)(\bar{\psi}\gamma_\mu\psi) \\ &- \frac{1}{2}\alpha_{TV}(\hat{\rho})(\bar{\psi}\vec{\tau}\gamma^\mu\psi)(\bar{\psi}\vec{\tau}\gamma_\mu\psi) \\ &- \frac{1}{2}\delta_S(\partial_v\bar{\psi}\psi)(\partial^v\bar{\psi}\psi) - e\bar{\psi}\gamma\cdot\mathbf{A}\frac{1-\tau_3}{2}\psi \end{aligned} \tag{6}$$

It contains the free-nucleon Lagrangian, the point-coupling interaction terms, and in addition to these two the model includes the coupling of the proton to the electromagnetic field. The derivative terms in Eq.(6) account for the leading effects of finite-range interactions that are crucial for a quantitative description of the nuclear properties. The functional form of the point-couplings chosen is

$$\alpha_i(\rho) = a_i + (b_i + c_i x)\, e^{-d_i x}, \qquad (i = S, V, TV) \tag{7}$$

where $x = \rho/\rho_{sat}$, and ρ_{sat} denotes the nucleon density at saturation in symmetric nuclear matter. In the present work, we have used the recently developed density-dependent point-coupling interaction DD-PC1 [40].

In the present investigation, the triaxial RHB with separable pairing model is used [46, 67]. In the presence of pairing the single-particle density matrix is generalized to two densities [68]: the normal density $\hat{\rho}$ and the pairing tensor $\hat{k}$. The RHB energy density functional is then given by:

$$E_{RHB}[\hat{\rho}, \hat{k}] = E_{RMF}[\hat{\rho}] + E_{pair}[\hat{k}], \tag{8}$$

where, $E_{RMF}[\hat{\rho}]$ is given by:

$$E_{RMF}[\psi, \bar{\psi}, \sigma, \omega^\mu, \vec{\rho^\mu}, A^\mu] = \int d^3r\mathcal{H} \tag{9}$$

and the $E_{pair}[\hat{k}]$ is given by:

$$E_{pair}[\hat{k}] = \frac{1}{4}\sum_{n_1 n_1^{'}}\sum_{n_2 n_2^{'}} k^*_{n_1 n_1^{'}}\langle n_1 n_1^{'}|V^{PP}|n_2 n_2^{'}\rangle k_{n_2 n_2^{'}}. \tag{10}$$

The index n refers to the original basis, and $< n_1 n_1^{'}|V^{PP}|n_2 n_2^{'} >$ are the matrix elements of the two-body pairing interaction. The effective interaction in the pp-channel, in $\mathbf{r}$-space has the form

$$V^{PP}(\mathbf{r_1}, \mathbf{r_2}, \mathbf{r_1'}, \mathbf{r_2'}) = -G\delta(\mathbf{R} - \mathbf{R}')P(\mathbf{r})\,P(\mathbf{r}') \tag{11}$$

where

$$\begin{aligned}\mathbf{R} &= \frac{1}{\sqrt{2}}(\mathbf{r_1} + \mathbf{r_2}) \\ \mathbf{r} &= \frac{1}{\sqrt{2}}(\mathbf{r_1} - \mathbf{r_2})\end{aligned} \tag{12}$$

being the center of mass and the relative coordinates, respectively. The form factor $P(\mathbf{r})$ is of the Gaussian shape

$$P(\mathbf{r}) = \frac{1}{(4\pi a^2)^{3/2}}e^{-r^2/2a^2}. \tag{13}$$

The two parameters G=728 MeV fm^3 and a=0.644 fm of this interaction are the same for protons and neutrons. It is derived in Ref. [69–72] by a mapping of the $^1S_0$ pairing gap of infinite nuclear matter to that of the Gogny force D1S [73].

The constrained calculations are performed by imposing constraints on both axial and triaxial mass quadrupole moments. The potential energy surface (PES) study as a function of the quadrupole deformation parameter is performed by the method of quadratic constraint [68]. The method of quadratic constraints uses an unrestricted variation of the function

$$\langle\hat{H}\rangle + \sum_{\mu=0,2} C_{2\mu}(\langle\hat{Q}_{2\mu}\rangle - q_{2\mu})^2 \tag{14}$$

where $\langle\hat{H}\rangle$ is the total energy, ($\langle\hat{Q_{2\mu}}\rangle$ denotes the expectation values of mass quadrupole operators,

$$\hat{Q}_{20} = 2z^2 - x^2 - y^2 \quad \text{and} \quad \hat{Q}_{22} = x^2 - y^2 \tag{15}$$

$q_{2\mu}$ is the constrained value of the multipole moment, and $C_{2\mu}$ is the corresponding stiffness constant [68]. Moreover, the quadratic constraint adds an extra force term $\sum_{\mu=0,2}\lambda_\mu\hat{Q}_{2\mu}$ to the system, where

$$\lambda_\mu = 2C_{2\mu}(\langle\hat{Q}_{2\mu}\rangle - q_{2\mu})^2 \tag{16}$$

for a self consistent solution. This term is necessary to force the system to a point in deformation space different from a stationary point. The augmented Lagrangian method [74] has also been implemented in order to resolve the problem of convergence of the self-consistent procedure which, diverges while increasing the value of stiffness constant $C_{2\mu}$ used in the procedure.

III. POTENTIAL ENERGY SURFACES

Potential energy surfaces (PES) have been calculated for Kr isotopes from neutron number N = 34 to 64 and for neutron rich Sr and Zr isotopes from neutron number N=48 to 70 in the (β, γ) plane. This is done systematically within the constrained triaxial calculations mapping the quadrupole deformation space defined by β_2 and γ using DD-ME2, NL3*, and DD-PC1 parametrizations. Contour plots have been made to investigate the location of a triaxial ground state, and the possible shape coexistence. The location of the ground state in the $\beta - \gamma$ deformation space is indicated by the point (β^0, γ^0).

A. Kr isotopes

Kr isotopes show a very rich structure and unusual shape coexistence phenomena in the ground state. In DD-PC1 results, one can notice that at the low end of the isotopic chain, that Kr isotopes have an axial oblate shape for N = 34. However, a very complex structure shows up for N = 36. In fact, four different minima can be found with energy difference less than 1 MeV. The global minimum is identical to the one in N = 34 case, but its location in the deformation space is shifted to larger β_2 deformation. Two of the remaining minima are triaxial one of them has $\gamma = 50$, $\beta_2 = 0.2$ and the other has $\gamma = 20$. $\beta_2 = 0.55$. The last minimum is prolate and located at $\beta_2 = 0.4$. It worth noting that there is a barrier of around 4 MeV in the middle of the PES separating the minima, two on each side of the barrier. As we move along the chain the minima merge with each other and we have only two minima for $^{74-78}$Kr isotopes, and then, between $^{80-88}$Kr, only one minimum is found, and it is spherical except the axial prolate shape for ^{82}Kr. Starting from ^{90}Kr (N = 54), the ground state starts to depart from spherical shape, and become deformed and soft in the γ direction. For ^{92}Kr (N = 56), the ground state is axially deformed and oblate. The ground state remains oblate up to the end of the isotopic chain. Shape coexistence manifest itself in the nuclei at either end of the isotopic chain, i.e. in $^{72-78,90-100}$Kr, with ^{94}Kr as the only exception. The result is very similar to the one we obtain with DD-ME2 parametrizations with two variations. These variations are seen in ^{84}Kr where we obtain a prolate axial ground state deformation instead of spherical ground state.

Shape evolution in Kr isotopes has been studied within the relativistic framework with BCS approximation for the pairing interaction using PC-PK1 parametrization in [23] which is a point coupling parametrization similar to the one we use, DD-PC1. However, DD-PC1 works much better for deformed nuclei, while PC-PK1 works better for spherical nuclei[65]. This difference in the both parametrization and pairing correlation lead to the difference in the bulk properties as will be seen later in the discussion. However, the authors of [23] studied only the neutron rich isotopes, $^{86-104}$Kr and missed the interesting features in the neutron deficient side of the chain shown in the PES of ^{72}Kr. Our results fully agree with the results presented in Ref.[23].

It was also studied within the interacting boson model (IBM) derived from the Gogny energy density functional [20]. The results with Gogny-D1M density functional and the mapped IBM shows very similar results to our calculations. However, they do not show the complex structure we have in ^{72}Kr. In addition, our results show a higher barrier between the minimum in ^{72,74}Kr.

In Tables I and II the list of the absolute minimum and the first excited minimum are listed for all the Kr isotopes under study. It is clear that the difference in energy between the two minima are less than 2.8 MeV.

TABLE I. Location of the two ground state minima indicated by (β^0, γ^0) for Kr isotopes using DD-PC1 parametrizations. The first minimum is the deepest minimum

Nucleus	1^{st} minimum	2^{nd} minimum	ΔE_{bin} (MeV)
^{70}Kr	(0.3,60^o)	-	N/A
^{72}Kr	(0.35,60^o)	(0.2,50^o)	1.1
^{74}Kr	(0.15,60^o)	(0.5,0^o)	0.5
^{76}Kr	Spherical	(0.2,60^o)	0.7
^{78}Kr	Spherical	(0.2,60^o)	0.7
^{80}Kr	Spherical	-	N/A
^{82}Kr	(0.15,0^o)	-	N/A
^{84}Kr	Spherical	-	N/A
^{86}Kr	Spherical	-	N/A
^{88}Kr	Spherical	-	N/A
^{90}Kr	(0.20,0^o − 60^o)	-	N/A
^{92}Kr	(0.25,60^o)	(0.25,0^o)	0.19
^{94}Kr	(0.30,60^o)	-	N/A
^{96}Kr	(0.35,60^o)	(0.45,0^o)	2.2
^{98}Kr	(0.30,60^o)	(0.40,0^o)	1.7
^{100}Kr	(0.30,60^o)	(0.40,0^o)	1.4

B. Sr and Zr isotopes

In Figs. 3 and 4 , we can see a sudden transition in ground state shape in the Sr chain, mainly as we move from ^{94}Sr (N = 56) to ^{96}Sr (N = 58). At the beginning of the chain, for $^{86-90}$Sr, the ground state minimum is spherical and there is no second minimum. However, moving along the chain, we encounter a triaxial ground state for ^{92,94}Sr according in the DD-PC1 calculations, but almost axial (oblate) with NL3*, but both parametrization do not predict a second minimum.

As we move along the chain and increase the neutron number, an emerging hill start to form and emerges from near $\beta_2 = 0$ and cause the existence of two new minima. Both of these minima are axial, but one of them is prolate and the other is oblate. The exact location of

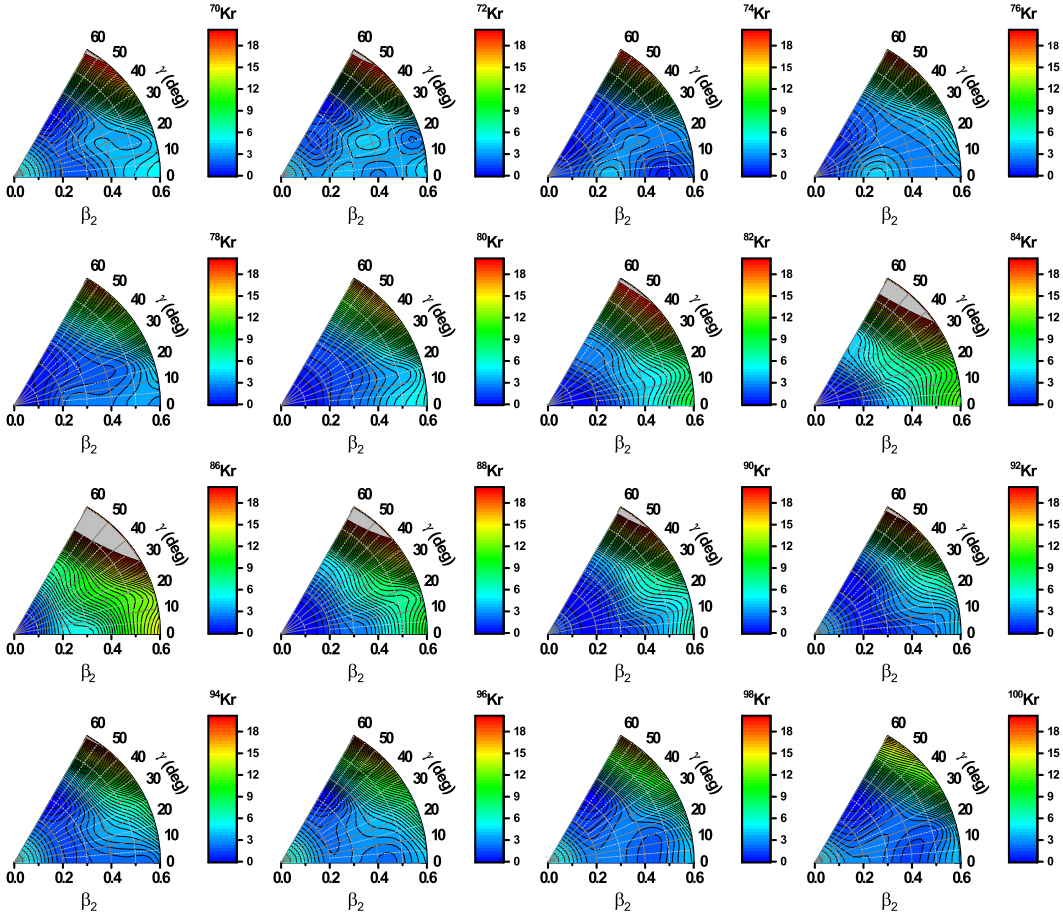

FIG. 1. (Color online) Potential energy surfaces of the Kr isotopes from neutron number $N = 34$ to 64 in the (β, γ) plane, obtained from a triaxial RHB calculations with the DD-PC1 parameter set. The color scale shown at the right has the unit of MeV, and scaled such that the ground state has a zero MeV energy.

TABLE II. Location of the two ground state minimum indicated by (β^0, γ^0) for Kr isotopes using DD-ME2 parameterizations. The first minimum is the deepest minimum

Nucleus	1^{st} minimum	2^{nd} minimum	ΔE_{bin} (MeV)
^{70}Kr	(0.3,60^o)	(0.25,0^o)	1.3
^{72}Kr	(0.35,60^o)	(0.2,40^o)	1.5
^{74}Kr	(0.15,60^o)	(0.35,60^o)	0.14
^{76}Kr	Spherical	(0.2,60^o)	0.64
^{78}Kr	Spherical	(0.2,60^o)	0.64
^{80}Kr	Spherical	-	N/A
^{82}Kr	(0.15,0^o)	-	N/A
^{84}Kr	(0.15,0^o)	-	N/A
^{86}Kr	Spherical	-	N/A
^{88}Kr	Spherical	-	N/A
^{90}Kr	(0.20,0^o − 60^o)	-	N/A
^{92}Kr	(0.25,60^o)	(0.25,0^o)	0.4
^{94}Kr	(0.30,60^o)	(0.45,0^o)	2.7
^{96}Kr	(0.35,60^o)	(0.45,0^o)	2.8
^{98}Kr	(0.30,60^o)	(0.40,15^o)	2.2
^{100}Kr	(0.30,60^o)	(0.45,5^o)	1.9

these two minima and the difference in energy is shown in Tables III and IV. For the NL3*, one can notice that from N = 56 up to N = 66, the oblate minimum is deeper than the prolate minimum with the energy difference less than 1.0 MeV. After that we can see that the ground state minimum becomes spherical and the difference in energy becomes more than 1.0 MeV and reaching a maximum value of 2.7 MeV for ^{108}Sr. Similar results are also obtained using the DD-PC1 parameter set. However, the main difference lies in the fact that DD-PC1 will always provide the first minimum to have an oblate shape and that the difference in energy between the two minima is less than 1 MeV in all of the cases specially for 106, 108Sr. Nevertheless, one can claim that the general trend of the results is independent from our choice of parametrizations, it is still noticeable that the size and height of the hill that developed for N = 58 are larger for the DD-PC1 results as compared with the NL3* results.

Softness in the γ - direction is clearer near the oblate minimum in the NL3* calculations. The existence of two ground state minima is present in Sr isotopes with neutron numbers greater than 54 and manifests itself at N = 60. Our results agree with the results presented in

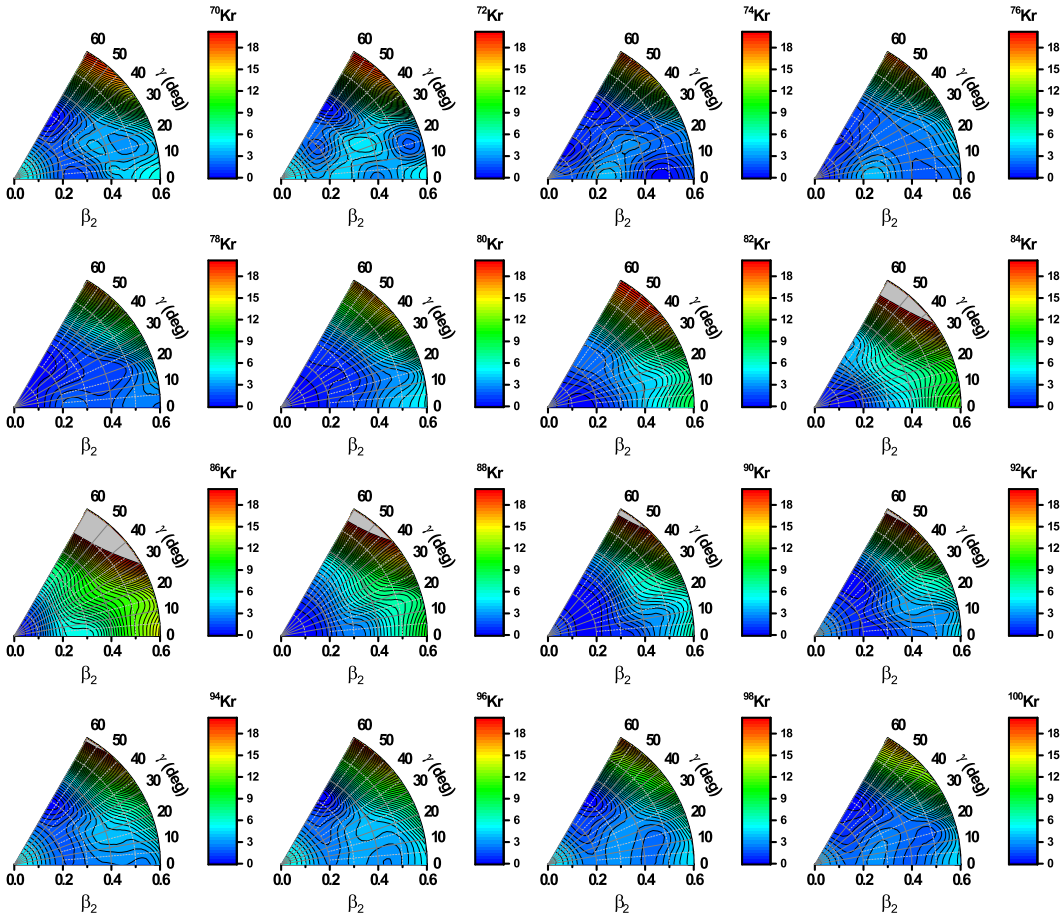

FIG. 2. (Color online) Potential energy surfaces of the Kr isotopes from neutron number $N = 34$ to 64 in the (β, γ) plane, obtained from a triaxial RHB calculations with the DD-ME2 parameter set. The color scale shown at the right has the unit of MeV, and scaled such that the ground state has a zero MeV energy.

TABLE III. Location of the two ground state minima indicated by (β^0, γ^0) for Sr isotopes using NL3* parametrizations. The first minimum is the deepest minimum

Nucleus	1^{st} minimum	2^{nd} minimum	ΔE_{bin} (MeV)
^{86}Sr	(0.0,0^o)	-	N/A
^{88}Sr	(0.0,0^o)	-	N/A
^{90}Sr	(0.0,0^o)	-	N/A
^{92}Sr	(0.15,55^o)	-	N/A
^{94}Sr	(0.20,60^o)	(0.4,0^o)	0.67
^{96}Sr	(0.50,0^o)	(0.25,60^o)	0.098
^{98}Sr	(0.45,0^o)	(0.35,60^o)	0
^{100}Sr	(0.45,0^o)	(0.30,55^o)	0.134
^{102}Sr	(0.20,60^o)	(0.45,0^o)	0.28
^{104}Sr	(0.15,60^o)	(0.45,0^o)	0.60
^{106}Sr	(0.0,0^o)	(0.45,0^o)	1.2
^{108}Sr	(0.0,0^o)	(0.45,0^o)	2.7

TABLE IV. Location of the two ground state minima indicated by (β^0, γ^0) for Sr isotopes using DD-PC1 parametrizations. The first minimum is the deepest minimum

Nucleus	1^{st} minimum	2^{nd} minimum	ΔE_{bin} (MeV)
^{86}Sr	(0.0,0^o)	-	N/A
^{88}Sr	(0.0,0^o)	-	N/A
^{90}Sr	(0.0,0^o)	-	N/A
^{92}Sr	(0.20,30^o)	-	N/A
^{94}Sr	(0.25,40^o)	(0.45,0^o)	0.03
^{96}Sr	(0.50,0^o)	(0.25,60^o)	0.94
^{98}Sr	(0.45,0^o)	(0.30,60^o)	0.65
^{100}Sr	(0.45,0^o)	(0.30,55^o)	0.86
^{102}Sr	(0.45,0^o)	(0.25,50^o)	0.68
^{104}Sr	(0.45,0^o)	(0.25,60^o)	0.24
^{106}Sr	(0.40,0^o)	(0.25,60^o)	0.53
^{108}Sr	(0.45,0^o)	(0.0,0^o)	0.40

[10], where the authors uses, a self-consistent mean-field approximation based on the D1S[77] interaction. In addition, our results are in agreement with other studies performed with the relativistic mean field approach[23] in predicting the shape evolution of the ground state with the NL3*. Our DD-PC1 results predict a prolate min-

imum in most of the cases. However, as we mentioned before the difference in energy between the prolate and oblate minimum is very small.

For the Zr (Z = 40) isotopic chain, the ground state for $^{88-92}$Zr are spherical and there is no secondary minimum. However, for ^{94,96}Zr the ground state is triaxial in both parametrizations. However, after that there is slight disagreement between the results from the the two parametrization.

As can be seen from Tables V and VI, one can see that NL3$*$ predict an oblate ground state for both ^{98,100}Zr and a prolate axial second minimum with an energy difference of less than 0.25 MeV. On the other hand DD-PC1 predicts the opposite, i.e. the ground state is prolate while the second minimum is oblate. Still the energy difference is considerably small and less than 1 MeV. Similarly, one notices similar behavior for ^{102,108,110}Zr, where the locations of the first and second minima are flipped in both parameterizations. However, they agree for ^{104,106}Zr.

This difference will not affect the binding energy and binding energy per nucleon, but will differently affect the neutron (proton) radius as will be shown later.

The major difference is that NL3* usually gives a higher difference as compared with DD-PC1. One of the minima is almost prolate and the other is almost oblate. It is interesting to see the existence of softness in the γ-direction. This softness comes in the shape of a belt that covers all the values of γ. However, as the barrier start to develop around $\beta_2 = 0.2$ it starts to split the belt into two separate regions and create two distinct minimum, a prolate and an oblate minimum. However, the splitting is stronger in the case of the DD-PC1 as compared with NL3*, and thus the existence of two shapes at ground state are more pronounced in the DD-PC1 results. Our results in both parametrizations agree with the results obtained in [23] where at the beginning of the chain the ground state shape is spherical then it becomes oblate and at the end of the chain it becomes spherical again.

The difference in energy between the two minima is less than 2 MeV in all of the cases and less than 1 MeV in the majority of them. Although, similar to the Sr isotopes results, the general trend of the evolution of the PES is independent of the type of parametrization. There are two interesting results that deserve a special discussion. ^{108,110}Zr. The NL3* results show two minima one of them is spherical and the other is oblate, and the difference in energy is 0.07 and 1.0 MeV, respectively. The DD-PC1 results are quite different. What really makes these two nuclei very interesting is the existence of a third minimum. The NL3* results indicate that this minimum is axially deformed and located at $\beta_2 = 0.45$ and it is prolate. Since there are some differences between both parametrizations in the ordering of the first and second minima, we can expect a slight difference in the location of the their minima in DD-PC1. The third minimum is for ^{108}Zr triaxial and located at $\beta_2 = 0.35$ and $\gamma = 30$, and is 0.93 MeV higher than the first minimum. For ^{110}Zr the first minimum is oblate and the second one is prolate, and not spherical. However, one can see an emerging minimum starts to develop at spherical shape for ^{110}Zr with an energy difference around 0.7 MeV and forms a third minimum. Thus, it is our belief that our result is independent from the choice of the parameter set, and that our finding is in complete agreement with the results of Ref. [10].

TABLE V. Location of the two ground state minima indicated by (β^0, γ^0) for Zr isotopes using NL3* parametrizations. The first minimum is the deepest minimum

Nucleus	1^{st} minimum	2^{nd} minimum	ΔE_{bin} (MeV)
^{88}Zr	(0.0,0^o)	-	N/A
^{90}Zr	(0.0,0^o)	-	N/A
^{92}Zr	(0.0,0^o)	-	N/A
^{94}Zr	(0.20,30^o)	-	N/A
^{96}Zr	(0.20,50^o)	(0.45,0^o)	1.25
^{98}Zr	(0.20,60^o)	(0.55,0^o)	0.09
^{100}Zr	(0.20,60^o)	(0.45,0^o)	0.25
^{102}Zr	(0.20,60^o)	(0.45,15^o)	0.54
^{104}Zr	(0.20,60^o)	(0.45,10^o)	0.90
^{106}Zr	(0.20,60^o)	(0.40,0^o)	1.0
^{108}Zr	(0.0,0^o)	(0.20,60^o)	0.07
^{110}Zr	(0.0,0^o)	(0.20,60^o)	1.0

TABLE VI. Location of the two ground state minima indicated by (β^0, γ^0) for Zr isotopes using DD-PC1 parametrizations. The first minimum is the deepest minimum

Nucleus	1^{st} minimum	2^{nd} minimum	ΔE_{bin} (MeV)
^{88}Zr	(0.0,0^o)	-	N/A
^{90}Zr	(0.0,0^o)	-	N/A
^{92}Zr	(0.0,0^o)	-	N/A
^{94}Zr	(0.20,30^o)	-	N/A
^{96}Zr	(0.20,45^o)	(0.45,0^o)	1.14
^{98}Zr	(0.55,0^o)	(0.25,60^o)	0.87
^{100}Zr	(0.55,0^o)	(0.25,60^o)	0.46
^{102}Zr	(0.40,15^o)	(0.25,60^o)	0.29
^{104}Zr	(0.25,55^o)	(0.4,10^o)	0.18
^{106}Zr	(0.20,60^o)	(0.40,0^o)	0.57
^{108}Zr	(0.25,60^o)	(0.40,0^o)	0.22
^{110}Zr	(0.20,60^o)	(0.40,0^o)	0.54

IV. PHYSICAL PROPERTIES

One can relate the shape evolution seen in the previous section with the change in the value of several physical properties of the ground state of these nuclei, namely, the binding energy (BE), proton radii (R_p) and neutron radii (R_n), two neutron separation energies (S_{2n}) and root mean square charge radii (R_c) with $\delta\langle r_c^2\rangle^{50,N} = \langle r_c^2\rangle^N - \langle r_c^2\rangle^{50}$.

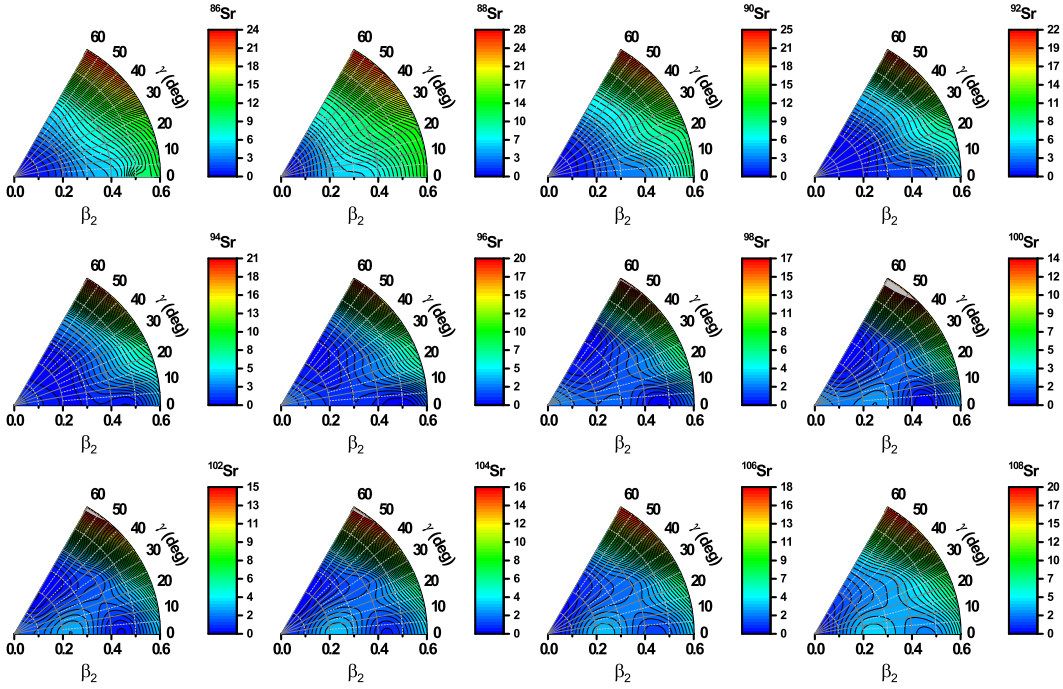

FIG. 3. (Color online) Potential energy surfaces of the Sr isotopes from neutron number $N = 48$ to 70 in the (β, γ) plane, obtained from a triaxial RHB calculations with the NL3* parameter set. The color scale shown at the right has the unit of MeV, and scaled such that the ground state has a zero MeV energy.

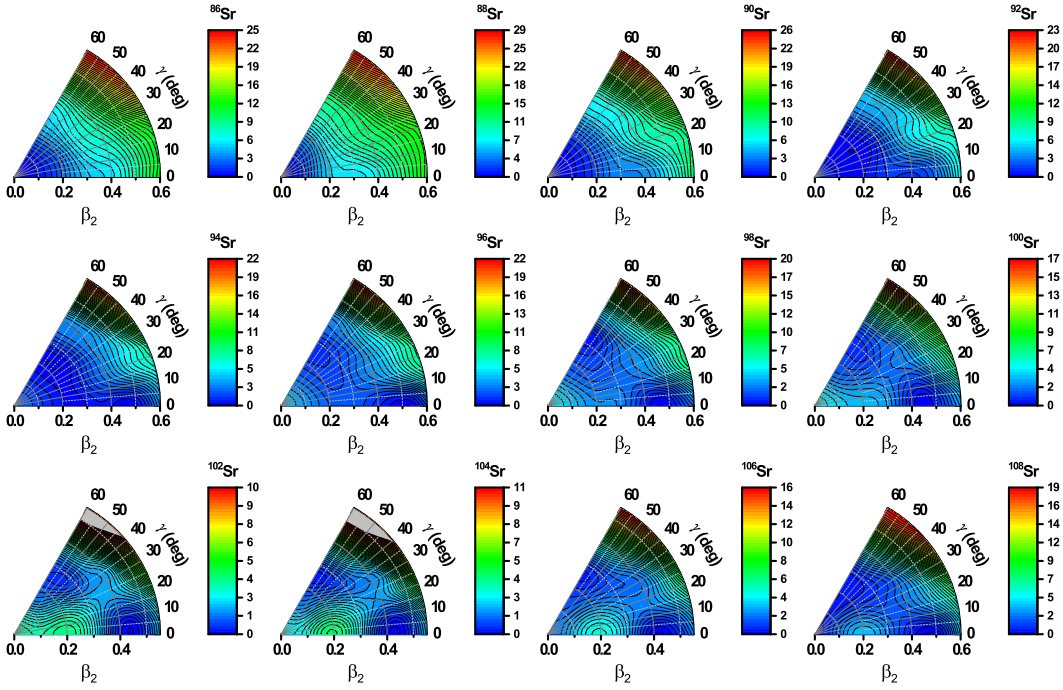

FIG. 4. (Color online) Same as in Fig. 3 but with DD-PC1.

The charge radius (R_c) is defined as

$$R_c = \sqrt{R_p^2 + 0.64} \tag{17}$$

where the 0.64 is a correction due to the finite size of the proton. A smooth transition in the ground state deformation will be seen as a smooth evolution of these properties. And a sudden change in the ground state deformation will be reflected as a sharp jump in these

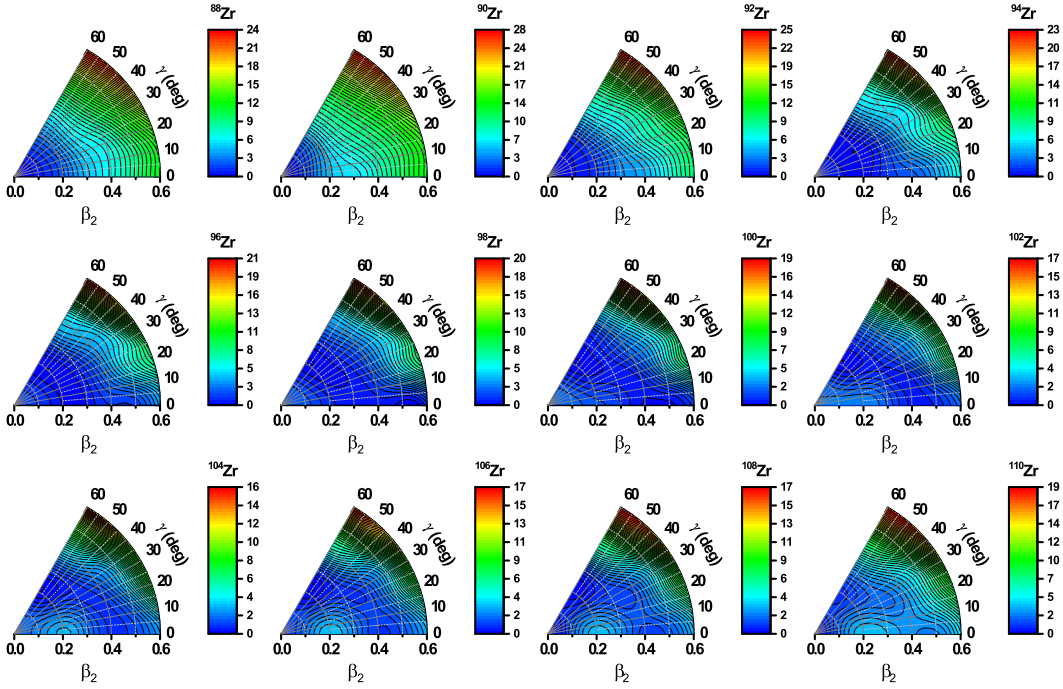

FIG. 5. (Color online) Potential energy surfaces of the Zr isotopes from neutron number $N = 48$ to 70 in the (β, γ) plane, obtained from a triaxial RHB calculations with the NL3* parameter set. The color scale shown at the right has the unit of MeV, and scaled such that the ground state has a zero MeV energy.

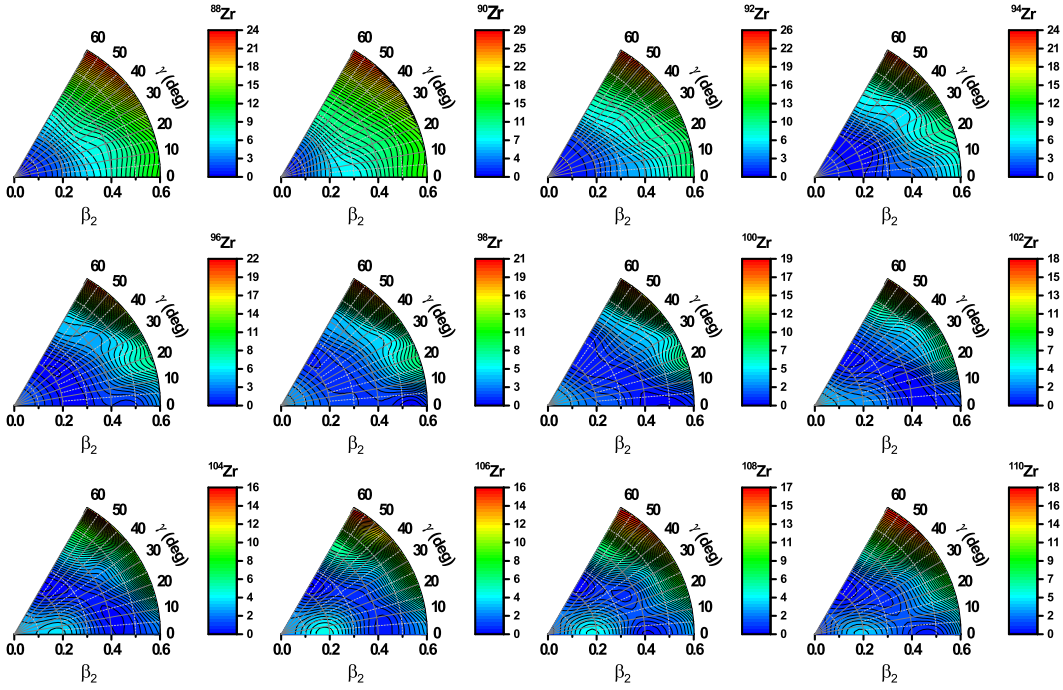

FIG. 6. (Color online) Same as in Fig. 5 but with DD-PC1

properties.

A. Kr isotopes

Our numerical results for the binding energy, binding energy per nucleon, and the two neutron separation en-

ergy (S_{2n}) for Kr isotopes are shown in Fig.7. Our results show very good agreement with experimental results and the results from FRDM and HFB based on D1S Gogny force. One exception can be found in the S_{2n} results at N = 52 , where our results show a sharp change. This is in agreement with the PES for Kr isotopes, specifically the transition between ^{88}Kr and ^{90}Kr corresponds to the change from spherical shape to a triaxial ground state with softness in the γ-direction.

There is a good agreement in Fig8.a for R_n values between our results and HFB results based on the Gogny-D1S. However, R_p, R_c and $\delta\langle r_c^2\rangle^{50,N} = \langle r_c^2\rangle^N - \langle r_c^2\rangle^{50}$ show a deviation from the HFB results. This is due to the fact that we predict a spherical shape for most of these nuclei, while they predict an oblate result. If we compare our results with the relativistic mean field calculations shown in Figure 6 in [23], then we will have a very good agreement with the values of the physical observable at the ground state minimum. It was mentioned in the previous section that our PES agrees with theirs.

There are no sudden changes in the ground state deformation along the Kr isotopic chain. This is well reflected in the behavior of the physical properties, which is smoothly changing with neutron number.

B. Sr and Zr isotopes

Theses results obtained in the previous sections are different from the ones obtained for Mo and Ru isotopes in [51]. It was shown that the shape transition along the isotopic chains was smooth, and that was reflected in the smooth evolution of the ground state properties. Thus, in the case of the Sr and Zr isotope chain, where there is a sudden transition in the ground state shape near the N = 60 shell gap one would expect a sharp change in the value of several physical properties of the ground state.

It is useful for our discussion to see the connection between figures of the PES and the tables of the location of the ground state minimum and the evolution of the physical observables at the ground state. To begin with we notice that there is a perfect agreement between our calculations using both NL3* and DD-PC1 and FRDM [75] and RMFT[76], which uses BCS approximation for pairing correlation, and HFB based on D1S Gogny force, for binding energy, the binding energy per nucleon and two neutron separation energy. It is worth noticing that the N = 50 shell gap is well pronounced and is directly related to the change of the slope of the two neutron separation energy S_{2n} shown in Fig. 12.

However, this agreement does not last, and we start to have fluctuations in the other quantities. For Sr isotopes the neutron and proton radius are shown in panels (a) and (b) of Fig. 13. One can notice that the sudden transition from spherical shape in the ground state to deformed shape in Sr isotopes is reflected in a sharp change in both neutron radius (R_n) and proton radius (R_p) at N = 56. NL3* predicts smaller values of R_p as compared

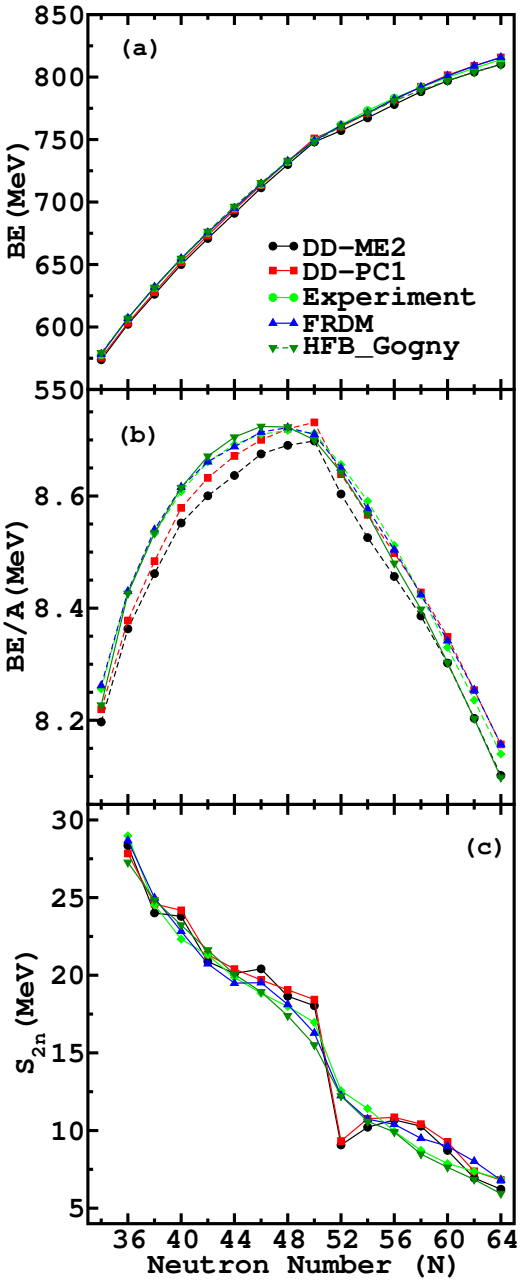

FIG. 7. (Color online) Binding energy, binding energy per nucleon and two neutron separation energy for Kr isotopes are shown in (a), (b) and (c) respectively. The results are shown using DD-PC1 and DD-ME2 as a function of neutron number. Comparison with FRDM [75] results, and HFB calculations based on the D1S Gogny force [77], and experimental data [78] are shown.

with the one obtained using DD-PC1 and other models. The main difference is coming from the fact that for $N \geq 64$ NL3* predicts a different location of the ground state minimum (i.e. different shape), but since the energy difference between the first and second minimum is very small this difference is not reflected in the behavior of the binding energy and related quantities. We notice

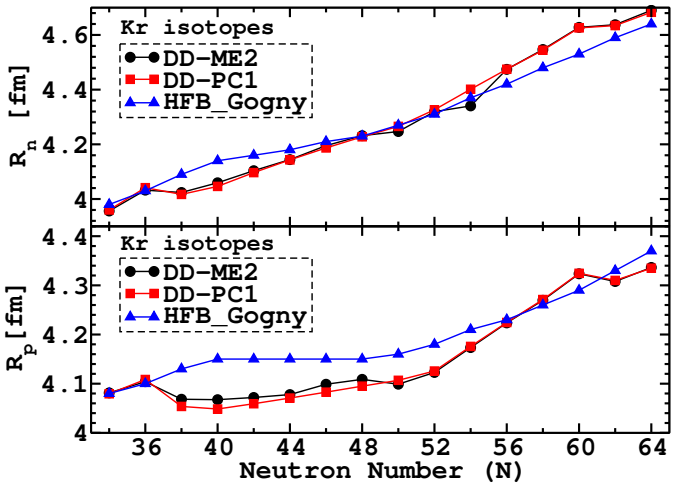

FIG. 8. (Color online) neutron radius (R_n) and proton radius (R_p)

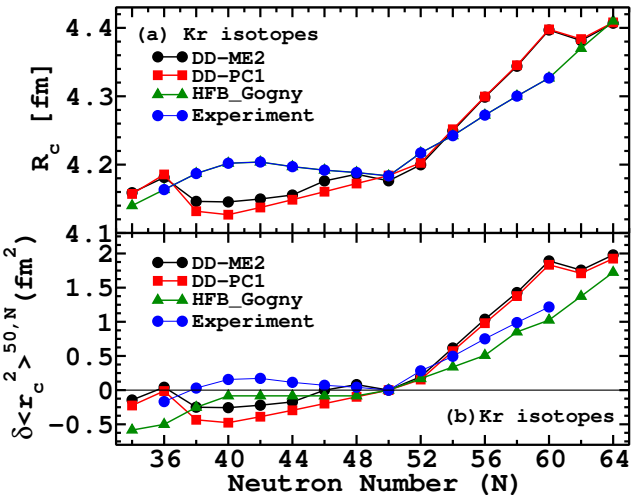

FIG. 9. (Color online) Charge radius (R_c).

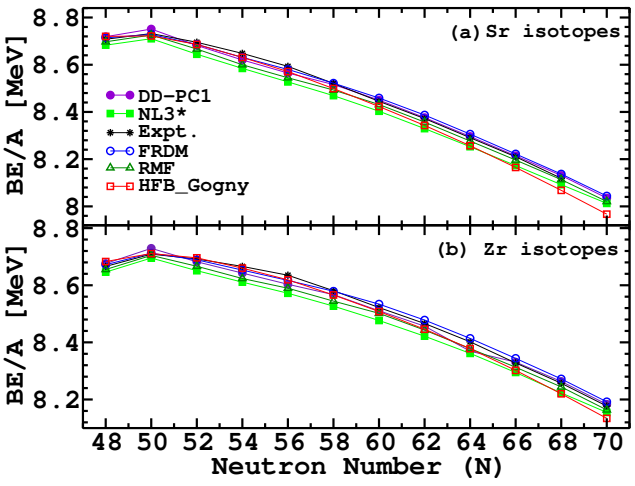

FIG. 10. (Color online) Binding energy per nucleon For Sr isotopes (a) and for Zr isotopes (b) using both NL3* and DD-PC1 as a function of neutron number. Comparison with FRDM [75] results, Relativistic Mean Field (RMF) model with NL3 functional [76], and HFB calculations based on the D1S Gogny force [77], and experimental data [78] are shown.

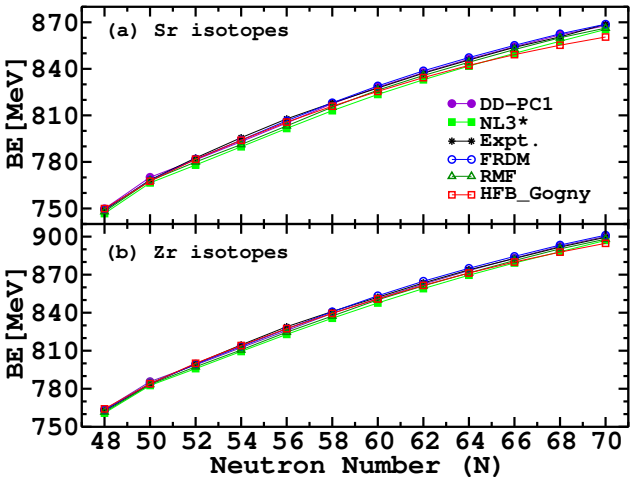

FIG. 11. Similar as Fig.10 but for total binding energy

that there is a decrease in both R_p and R_c in the NL3* calculations, this is due to the fact that it predicts either an oblate axial or a spherical ground state while DD-PC1 predicts a prolate axial ground state deformation.

We can also compare the charge radius of Sr isotopes with the results shown in Figure 5.b in Ref.[82], which can be found to agree with our results with DD-PC1. Both of them find the ground state to be prolate along the end of the isotopic chain. The values obtained with NL3* agrees with the oblate results shown in Fig. 5.b in Ref.[82].

Similarly, one can see that for Zr isotopes the deviation is restricted to only two nuclei, with N = 58 and 60. These two nuclei have different ground states in both parametrizations. It is also interesting to see that there is a decrease in R_p values of Zr isotopes using DD-PC1, for N = 60-66. This can be related to the fact that the value of β_2 deformation for the ground state decreases along these nuclei. If one uses the R_p values at the same deformation as in $NL3^*$ then we will get very similar results. The rest of the chain isotopes follow the same trend as the other models. The charge radius R_c, shown in Fig. 14, and $\delta\langle r_c^2\rangle^{50,N}$, shown in Fig. 15, behave in a similar fashion to R_p and show the same type of deviation.

Although there is some deviation between our calculations and the results obtained in experiments and other models in some of the nuclei, due to the different prediction of the ground state minimum, it is still safe to say that our results show in general the same trend as other models and agrees with them.

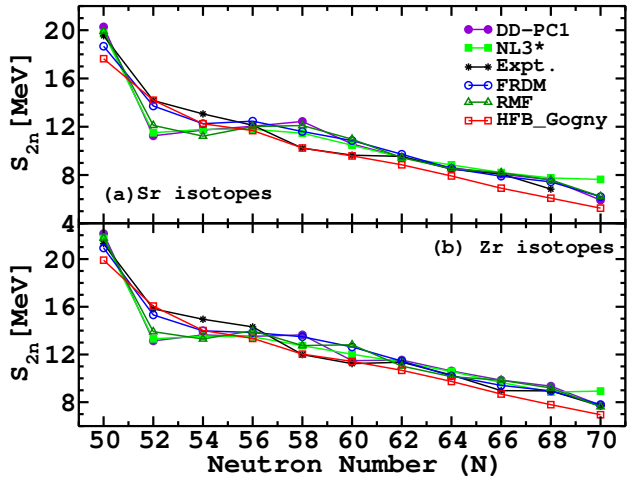

FIG. 12. Similar as Fig.10 but for two-neutrons separation energy (S_{2n})

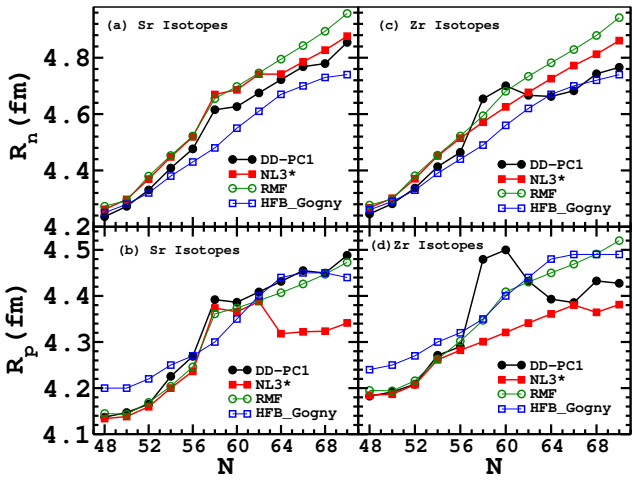

FIG. 13. Neutron radius (R_n) and proton radius R_p For Sr isotopes and for Zr isotopes using both NL3* and DD-PC1 as a function of neutron number. Comparison with Relativistic Mean Field (RMF) model with NL3 functional [76], and HFB calculations based on the D1S Gogny force [77] are shown.

V. CONCLUSION

We have used the Relativistic-Hartree-Bogoliubov (RHB) formalism with separable pairing to perform a systematic calculation along three isotopic chains, Kr, Sr, and Zr, to investigate the triaxial ground state, the phenomena of unusual structural change and the coexistence of shape. Our results indicated that shape transition is smooth for the Kr isotopes. On the other side the shape evolution in Zr and Sr isotopes is not smooth , but rather sudden. This is well reflected in the behavior of physical observables such as the proton and neutron radii as well as the two neutron separation energies. ^{72}Kr and ^{108,110}Zr show a complicated PES structure, four and three minima, respectively. One can see the existence of three minima, while all other nuclei show only two.

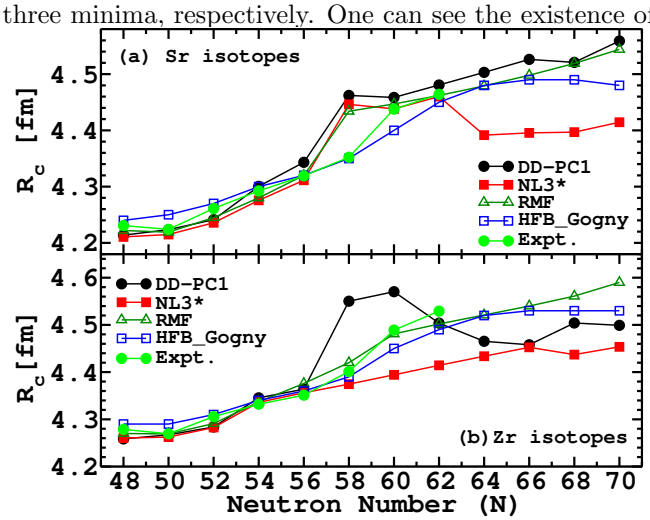

FIG. 14. Charge radius R_c For Sr isotopes and for Zr isotopes using both NL3* and DD-PC1 as a function of neutron number. Comparison with Relativistic Mean Field (RMF) model with NL3 functional [76], and HFB calculations based on the D1S Gogny force [77] and experimental data [79] are shown.

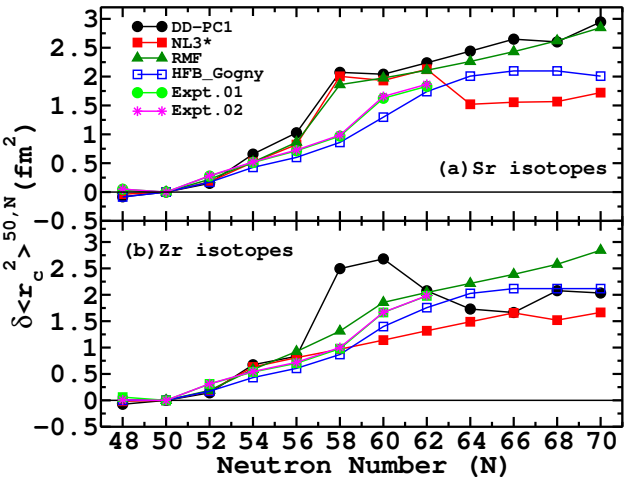

FIG. 15. $\delta\langle r_c^2\rangle^{50,N}$ for Sr and Zr isotopes as a function of neutron numbers. Experimental data are taken from [79–81]

Our overall results show independence from the choice of parameterizations, and in good agreement with results obtained from different models. It agrees with the results obtained in FRDM [75], Relativistic Mean Field (RMF) model with NL3 functional [23, 76], and HFB calculations based on the D1S Gogny force [77].

[1] E. Cheifetz, *et al.*, Phys. Rev. Lett. **25**, 38 (1970).

[2] H. Mach, *et al.*, Phys. Lett. B **230**, 21 (1989).

[3] A. N. Andreyev, *et al.*, Nature (London) **405**, 430 (2000).
[4] J. D. Cole, *et al.*, Phys. Rev. Lett. **37**, 1185 (1976).
[5] E. Bouchez, *et al.*, Phys. Rev. Lett. **90**, 082502 (2003).
[6] N. Bree, *et al.*, Phys. Rev. Lett. **112**, 162701 (2014).
[7] E. Clément, *et al.*, Phys. Rev. C **75**, 054313 (2007).
[8] S. Naimi, *et al.*, Phys. Rev. Lett. **105**, 032502 (2010).
[9] M. Albers *et al.*, Phys. Rev. Lett. **108**, 062701 (2012).
[10] R. Rodríguez-Guzmán, P. Sarriguren, L. M. Robledo, S. Perez-Martin, Phys. Lett. B **691**, 202 (2010).
[11] K. Heyde and J. L. Wood, Rev. Mod. Phys. **83**, 1467 (2011).
[12] E. Clément, *et al.*, Phys. Rev. Lett. **116**, 022701 (2016).
[13] A. Chakraborty, *et al.*, Phys. Rev. Lett. **110**, 022504 (2013).
[14] C. Y. Wu, H. Hua, D. Cline, A. B. Hayes, R. Teng, R. M. Clark, P. Fallon, A. Goergen, A. O. Macchiavelli, and K. Vetter, Phys. Rev. C **70**, 064312 (2004).
[15] J. L. Wood, K. Heyde, W. Nazarewicz, M. Huyse, and P. van Duppen, Phys. Rep. **215**, 101 (1992).
[16] J. L. Wood, E. F. Zganjar, C. De Coster, and K. Heyde, Nucl. Phys. A **651**, 323 (1999).
[17] C. Y. Wu, H. Hua, and D. Cline, Phys. Rev. C **68**, 034322 (2003).
[18] G. Lhersonneau, *et al.*, Phys. Rev. C **49**, 1379 (1994).
[19] K. Nomura, R. Rodríguez-Guzmán, and L. M. Robledo, Phys. Rev. C **94**, 044314 (2016).
[20] K. Nomura, R. Rodríguez-Guzmán, Y. M. Humadi, L. M. Robledo and H. Abusara, Phys. Rev. C **96**, 034310 (2017)
[21] A. Petrovici, Phys. Rev. C **85**, 034337 (2012).
[22] K. Sieja, F. Nowacki, K. Langanke, and G. Martínez-Pinedo, Phys. Rev. C **79**, 064310 (2009).
[23] J. Xiang, Z.P. Li, Z.X. Li, J.M. Yao, and J. Meng, Nucl. Phys. A **873**, 1 (2012).
[24] G. Lalazissis and M. M. Sharma, Nucl. Phys. A **586**, 201 (1995).
[25] H. Zhang, S. Im, J. Li, W. Zuo, Z. Ma, B. Chen, and W. Scheid, Eur. Phys. J. A **30**, 519 (2006).
[26] J. Skalski, S. Mizutory, and W. Nazarewicz, Nucl. Phys. A **617**, 282 (1997).
[27] J. E. García-Ramos *et al.*, Eur. Phys. J. A **26**, 221 (2005).
[28] A. Petrovici, K. W. Schmid, and A. Faessler, J. Phys. **312**, 092051 (2011).
[29] A. Petrovici, K. W. Schmid, and A. Faessler, Prog. Part. Nucl. Phys. **66**, 287 (2011).
[30] P. G. Reinhard, D. J. Dean, W. Nazarewicz, J. Dobaczewski, J. A. Maruhn, and M. R. Strayer, Phys. Rev. C **60**, 014316 (1999).
[31] A. Holt, T. Engeland, M. Hjorth-Jensen, and E. Osnes, Phys. Rev. C **61**, 064318 (2000).
[32] Y.-X. Liu, *et al.*, Nucl. Phys. A **858**, 11 (2011).
[33] P. Federman and S. Pittel, Phys. Rev. C **20**, 820 (1979).
[34] A. Kumar and M. R. Gunye, Phys. Rev. C **32**, 2116 (1985).
[35] T. Rzaca-Urban, K. Sieja, W. Urban, F. Nowacki, J. L. Durell, A. G. Smith, and I. Ahmad, Phys. Rev. C **79**, 024319 (2009).
[36] S. Michiaki and A. Akito, Nucl. Phys. A **515**, 77 (1990).
[37] A. Baran and W. Höhenberger, Phys. Rev. C **52**, 2242 (1995).
[38] H. Mei, J. Xiang, J. M. Yao, Z. P. Li, and J. Meng, Phys. Rev. C **85**, 034321 (2012).
[39] C. Özen and D. J. Dean, Phys. Rev. C **73**, 014302 (2006).
[40] T. Nikšić, D. Vretenar, and P. Ring, Phys. Rev. C **78**, 034318 (2008).
[41] G. A. Lalazissis, S. Karatzikos, R. Fossion, D. Peña Arteaga, A. V. Afanasjev, and P. Ring, Phys. Lett. B **671**, 36 (2009).
[42] S. E. Agbemava, A. V. Afanasjev, D. Ray, and P. Ring, Phys. Rev. C, **89**, 054320 (2014).
[43] S. E. Agbemava, A. V. Afanasjev, D. Ray, and P. Ring, Phys. Rev. C, **95**, 054324 (2017).
[44] A. V. Afanasjev and S. E. Agbemava, Phys. Rev. C **93**, 054310 (2016).
[45] S. E. Agbemava, A. V. Afanasjev, T. Nakatsukasa, and P. Ring, hys. Rev. C **92**, 054310 (2015).
[46] T. Nikšić, N. Paar, D. Vretenar, and P. Ring, Comp. Phys. Comm. **185**, 1808 (2014).
[47] G. A. Lalazissis, T. Nikšić, D. Vretenar, and P. Ring, Phys. Rev. **C71**, 024312 (2005).
[48] T. Nikšić, D. Vretenar, P. Finelli, and P. Ring, Phys. Rev. C **66**, 024306 (2002).
[49] X. Roca-Maza, X. Viñas, M. Centelles, P. Ring, and P. Schuck, Phys. Rev. C **84**, 054309 (2011).
[50] N. Paar , D. Vretenar , E. Khan and G. Coló, Rep. Prog. Phys. **70**, 691 (2007).
[51] H. Abusara, Shakeb Ahmad, and S. Othman, Phys. Rev. C **95**, 054302 (2017).
[52] Afaque Karim, Shakeb Ahmad, Phys. Rev. C **92**, 064608 (2015).
[53] H. Abusara, A. V. Afanasjev, and P. Ring, Phys. Rev. C **85**, 024314 (2012).
[54] T. Nikšić, D. Vretenar, and P. Ring, Prog. Part. Nucl. Phys. **66**, 519 (2011).
[55] A. V. Afanasjev and H. Abusara, Phys. Rev. C **81**, 014309 (2010).
[56] D. Vretenar, A. V. Afanasjev, G. A. Lalazissis, and P. Ring, Phys. Rep. **409**, 101 (2005).
[57] Y. K. Gambhir, P. Ring, and A. Thimet, Ann. Phys. (NY) **198**,132 (1990).
[58] B.B.Serot and J.D.Walecka, *Advances of Nuclear Physics*, edited by J. W. Negle and E. Vogt,Vol.**16**(Planum, New York, 1986).
[59] J. D. Walecka, Ann. Phys. (NY) **83**, 491 (1974).
[60] J. Boguta and A. R. Bodmer, Nucl. Phys. A **292**, 413 (1977).
[61] W. Pannert, P. Ring, and J. Boguta, Phys. Rev. Lett.**59**, 2420 (1987).
[62] P. G. Reihard, M. Rufa, J. Maruhn, W. Greiner, J. Friedrich, Z. Phys. A **323** (1986).
[63] G. A. Lalazissis, J. König, P. Ring, Phys. Rev. C **55**, 540 (1997).
[64] B. G. Todd-Rutel, J. Piekarewicz, Phys. Rev. Lett. **95**, 122501 (2005).
[65] P. W. Zhao, Z. P. Li, J. M. Yao, J. Meng, Phys. Rev. C **82**, 054319 (2010).
[66] B. A. Nikolaus, T. Hoch, and D. G. Madland, Phys. Rev. C **46**, 1757 (1992).
[67] P.Ring, Prog.Part.Nucl.Phys.**37**,193(1996).
[68] P. Ring and P. Schuck,*The Nuclear Many-Body Problem*, eds. W. Beiglbck *et al.* (New York, Springer-Verlag), (1980).
[69] Y. Tian, Z. Y. Ma, P. Ring, Phys. Lett. B **676**, 44 (2009).
[70] Y. Tian, Z. Y. Ma, P. Ring, Phys. Rev. C **79**, 064301 (2009).
[71] Y. Tian, Z. Y. Ma, P. Ring, Phys. Rev. C **80**, 024313 (2009).

[72] T. Nikšić, P. Ring, D. Vretenar, Y. Tian, Z. Y. Ma, Phys. Rev. C **81**, 054318 (2010).
[73] J. F. Berger, M. Girod, D. Gogny, Comput. Phys. Comm. **63**, 365 (1991).
[74] A. Staszack, M. Stoitsov, A. Baran, W. Nazarewicz, Eur. Phys. J. A **46**, 85 (2010).
[75] P. Möller, J.R. Nix, K.-L. Kratz, At. Data Nucl. Data Tables **66**, 131 (1997).
[76] G.A. Lalazissis, S. Raman, P. Ring, At. Data Nucl. Data Tables 71, 1 (1999)
[77] $http://www-phynu.cea.fr/HFB-Gogny_eng.htm.$
[78] M. Wang, G. Audi, A.H. Wapstra et al., Chin. Phys. C **36**, 1603 (2012).
[79] I. Angeli, K.P. Marinova, At. Data Nucl. Data Table 99, 69 (2013)
[80] F. Buchinger, et al., Phys. Rev. C 41, 2883 (1990).
[81] P. Campbell, et al., Phys. Rev. Lett. 89, 082501 (2002)
[82] P. Sarriguren Phys. Rev. C 91, 044304 (2015)